

Relativistic mask method for electron momentum distributions after ionization of hydrogen-like ions in strong laser fields

D. A. Tumakov,^{1,*} Dmitry A. Telnov,^{1,†} G. Plunien,² V. A. Zaytsev,¹ and V. M. Shabaev¹

¹*Department of Physics, St. Petersburg State University,
Universitetskaya Naberezhnaya 7/9, St. Petersburg 199034, Russia*

²*Institut für Theoretische Physik, Technische Universität Dresden, Mommsenstrasse 13, Dresden D-01062, Germany*

Wavefunction-splitting or mask method, widely used in the non-relativistic calculations of the photoelectron angular distributions, is extended to the relativistic domain within the dipole approximation. Since the closed-form expressions for the relativistic Volkov states are not available within the dipole approximation, we build such states numerically solving a single second-order differential equation. We calculate the photoelectron energy spectra and angular distributions for highly charged ions under different ionization regimes with both the direct and the relativistic mask methods. We show that the relativistic mask method works very well and reproduces the electron energy and angular distributions calculated by the direct method in the energy range where both methods can be used. On the other hand, the relativistic mask method can be applied for longer laser pulses and/or higher photoelectron energies where the direct method may have difficulties.

PACS numbers: 32.80.Fb, 31.30.Jv

I. INTRODUCTION

With recent advancement of the laser technologies making it possible to generate extremely intense short pulses, the light-matter interaction phenomena draw much attention both in the theory and experiment [1–4]. The most powerful free-electron laser facilities, such as XFEL [5] at Hamburg and LCLS [6] at Stanford, are expected to produce electromagnetic fields with the peak brilliance of up to 5×10^{33} photons/s/mm²/mrad²/0.1% bandwidth and wavelengths down to 0.05 nm. Such extremely strong and high-frequency fields take the electronic dynamics of the target to the relativistic domain. Interaction of these fields with highly-charged ions is of particular interest, given the fact that such ions have their own strong Coulomb fields where the electronic motion is essentially relativistic. In this respect, we should mention the shortly upcoming High-Intensity Laser Ion-Trap Experiment (HILITE) experiment [7–9], which is intended to study the light-matter interaction using the Penning trap.

For the correct theoretical description of such processes, a relativistic treatment should be invoked to capture the electron dynamics: not only the bound electron is relativistic for the ions with high nucleus charge Z , but also the ionized electrons can reach the relativistic velocities. Various approaches exist today, including relativistic extensions of the strong field approximation (SFA) [10], numerical solution of the 3D Dirac equation [11–18], and the modification of the Schrödinger equation allowing to account for relativistic effects to a large extent [19].

Photoelectron angular and energy distributions contain various information about both the ionization process and internal structure of the target. Besides the familiar above-threshold ionization (ATI) peaks [20] and rescattering

plateau [21] they can feature many subtle effects: “channel-closing” [22, 23], Stark-induced Rydberg states resonances (Freeman resonances) [24, 25], low energy structure (LES) attributed to the Coulomb focusing effect [26, 27], or interference structure originating from interfering electrons, emitted at different times [28–34]. Advances in the experimental setups draw a lot of attention to these fine structures and effects present in the electron spectra.

For the direct calculation of the photoelectron angular distributions (PAD) in the relativistic regime one has to solve the full-dimensional time-dependent Dirac equation numerically. However, this solution is computationally expensive, especially if the ionized wavepacket travels a long distance from the ionic core. There are a number of non-relativistic well-established methods to extract the PAD without the full information about the wave packet in remote regions of the space: the window operator technique [35]; geometrical splitting of the coordinate space and the wavefunction (mask method) [36–38], which can be directly connected to the usage of complex absorbing potentials (CAPs) or smooth exterior complex scaling [39]; description of the electron dynamics in the Kramers-Henneberger reference frame [40, 41]; calculation of the flux through a spherical surface placed far enough from the core [42], and the solution of the dynamical equations in the momentum representation [43, 44].

In this contribution, we introduce the relativistic generalization of the mask method for the hydrogen-like ions and provide its numerical illustrations studying the ionization of such ions by strong linearly-polarized laser pulses. Since the method is based on the Dirac equation, it enables a correct and natural treatment of the relativistic electronic structure of highly-charged ions. The method can be used to obtain the PAD without propagation of the wave function to long times and large distances for the hydrogen-like system, and can also be directly generalized to the many-electron problems within the density functional theory framework. The present formulation of the method is restricted to the dipole approximation for the interaction of the electron with the electromagnetic field. With increasing the field intensity the dipole ap-

* dm.tumakov@gmail.com

† d.telnov@spbu.ru

proximation will eventually break down. Depending on the wavelength, the applicability of this approximation may become questionable even for the fields which are not extremely strong. This issue has been widely discussed in the literature (see, for example, Refs. [45–49]). We should mention two different aspects here. First, applicability of the dipole approximation is limited to the radiation wavelengths which are much larger than the size of the target, so the spatial dependence of the field can be safely ignored. The second limitation is related to the influence of the magnetic field component on the electronic motion, which is more significant for stronger fields and faster electrons. When the nondipole effects become important, the method presented in this paper cannot be used for accurate evaluation of the photoelectron distributions. However, it still can be used to estimate the magnitude of the nondipole corrections. To do so one has to compare the dipole and nondipole results, thus the calculations within the dipole approximation make sense even in the case when this approximation is not very accurate. Still, a wide range of photon energies and field intensities exists where the dipole approximation is expected to work reasonably well. In our case studies, we use the field parameters where the dipole approximation is well justified.

The paper is organized as follows. In Sec. II we describe in detail the theoretical and computational methods applied to the present problem. The examples of the method implementation, the results of our calculations, and all necessary theoretical analyses are presented in Sec. III. Sec. IV contains the concluding remarks. Atomic units are used throughout the paper ($\hbar = m_e = |e| = 1$), unless specified otherwise.

II. THEORETICAL AND COMPUTATIONAL METHODS

A. Hydrogen-like ion exposed to a strong laser field

Relativistic dynamics of the electron in a hydrogen-like ion is governed by the time-dependent Dirac equation (TDDE):

$$i \frac{\partial}{\partial t} \Psi(\mathbf{r}, t) = [H_0 + V(\mathbf{r}, t)] \Psi(\mathbf{r}, t), \quad (1)$$

where the stationary part of the Hamiltonian reads

$$H_0 = c\boldsymbol{\alpha} \cdot \mathbf{p} + c^2\beta + V_{\text{nuc}}, \quad (2)$$

with $c \approx 137$ being the speed of light; $\boldsymbol{\alpha}$ and β are the Dirac matrices. Spherically-symmetric potential V_{nuc} describes the interaction with the nucleus:

$$V_{\text{nuc}} = -\frac{Z(r)}{r}, \quad (3)$$

where $Z(r)$ is the effective nuclear charge. In all our calculations we use the model of a charged sphere for the nucleus with nuclear radii taken from Ref. [50]. We consider the interaction with the external electromagnetic field of the laser pulse within the dipole approximation in the velocity gauge, so the interaction term reads

$$V(\mathbf{r}, t) = c\boldsymbol{\alpha} \cdot \mathbf{A}(t) \quad (4)$$

with the “vector potential” defined as $\mathbf{A}(t) = -\int_{-\infty}^t \mathbf{F}(\tau) d\tau$, where $\mathbf{F}(\tau)$ is the electric field strength. We assume the electric field to be a linearly-polarized laser pulse along the z axis with sine-squared envelope for the vector potential:

$$\mathbf{A}(t) = \begin{cases} -\frac{F}{\omega} \mathbf{e}_z \sin^2 \frac{\omega t}{2N} \sin \omega t & (0 \leq t \leq T), \\ 0 & (t < 0, t > T), \end{cases} \quad (5)$$

where ω and F are the carrier frequency and the peak field strength, respectively, N denotes the number of optical cycles, and $T = \frac{2\pi N}{\omega}$ is the pulse duration.

Since the full Hamiltonian is axially-symmetric, the initial projection $m = 1/2$ of the electron total angular momentum j on z axis is conserved during the interaction. Utilizing this fact we can factor out the dependence on the angle φ (rotation angle about the z -axis) in the wavefunction explicitly, reducing the problem’s dimension:

$$\Psi(\mathbf{r}, t) = \frac{1}{\sqrt{2\pi r}} \begin{pmatrix} \psi_1(r, \theta, t) \\ e^{i\varphi} \psi_2(r, \theta, t) \\ i\psi_3(r, \theta, t) \\ ie^{i\varphi} \psi_4(r, \theta, t) \end{pmatrix}. \quad (6)$$

The four-component function $\psi(r, \theta, t)$ formed by the scalar functions $\psi_i(r, \theta, t)$ satisfies the following equation:

$$i \frac{\partial}{\partial t} \psi(r, \theta, t) = \tilde{H}(t) \psi(r, \theta, t), \quad (7)$$

where

$$\tilde{H}(t) = \begin{pmatrix} (V_{\text{nuc}} + c^2) \cdot \mathbf{1}_2 & c(D + iA_z(t)\sigma_z) \\ -c(D + iA_z(t)\sigma_z) & (V_{\text{nuc}} - c^2) \cdot \mathbf{1}_2 \end{pmatrix} \quad (8)$$

and

$$D = (\sigma_x \sin \theta + \sigma_z \cos \theta) \left(\frac{\partial}{\partial r} - \frac{1}{r} \right) + \frac{1}{r} (\sigma_x \cos \theta - \sigma_z \sin \theta) \frac{\partial}{\partial \theta} + \frac{1}{2r \sin \theta} (\sigma_x + i\sigma_y) \quad (9)$$

with σ_x , σ_y , and σ_z being the Pauli matrices, and $\mathbf{1}_2$ being the 2×2 unity matrix.

To obtain the initial state for the time-dependent problem (7) we consider first the time-independent Dirac equation for the electron in a hydrogen-like ion:

$$\tilde{H}(t=0) \phi_n = \varepsilon_n \phi_n. \quad (10)$$

The problem (10) can be solved numerically with the straightforward implementation of the generalized pseudospectral (GPS) method (for the details, see, for example, [14, 51, 52]). Discretization of the Eq. (10) leads to the symmetric matrix eigenvalue problem, which can be solved efficiently with the linear algebra routines.

It is well-known that solution of the stationary Dirac equation with finite basis sets leads to the emergence of the non-physical spurious states in the spectrum [53, 54]. In our calculations, such states emerge and move upwards in the spectrum

with the size of the basis set increase. We have checked, however, that the occurrence of such states does not affect the final results, since the transition probabilities are negligibly small for them.

To solve the Eq. (7) we implement the time-dependent generalized pseudospectral (TDGPS) method [55], which was successfully employed in many previous calculations [14, 56, 57] for the Dirac equation. The four-component function $\psi(r, \theta, t)$ is discretized on the two-dimensional GPS grid (see Ref. [14] for details) and propagated in time by the Crank-Nicolson (CN) propagation scheme [58]:

$$\begin{aligned} & \left[1 + \frac{i\Delta t}{2} \tilde{H} \left(t + \frac{\Delta t}{2} \right) \right] \psi(r, \theta, t + \Delta t) \\ &= \left[1 - \frac{i\Delta t}{2} \tilde{H} \left(t + \frac{\Delta t}{2} \right) \right] \psi(r, \theta, t), \end{aligned} \quad (11)$$

with the initial condition set to be the ion ground state:

$$\psi(r, \theta, t = 0) = \phi_{1s}(r, \theta). \quad (12)$$

A set of the linear equations (11) should be solved on each propagation step, which can be quite time-consuming, especially for extremely strong laser fields. However, the CN method allows the time step to be relatively large for obtaining converged results [57]. In addition, the matrix of the Hamiltonian $\tilde{H}(t)$ is very sparse within the GPS discretization (given that almost always the size of the angular grid is much smaller than the radial one); in all our calculations the number of non-zeros in Hamiltonian matrix is around 3%. These facts allow one to implement the scheme (11) very efficiently using the existing libraries for the iterative solution of the linear equations with sparse matrices. In the present study we make use of the Intel® MKL PARDISO [59] library.

B. Direct PAD evaluation

Having the full wavefunction at time $\tau > T$ after laser pulse is switched off, the momentum distribution of the photoelectrons can be obtained directly as

$$\frac{d^2 P(\mathbf{k})}{dE d\Omega} = \frac{k}{c^2} E \sum_{\mu} |\langle \Psi_{\mathbf{k}\mu}^-(\mathbf{r}) | \Psi(\mathbf{r}, \tau) \rangle|^2. \quad (13)$$

Continuum wavefunction $\Psi_{\mathbf{k}\mu}^-(\mathbf{r})$ of the unperturbed Hamiltonian describes the electron state with the asymptotic momentum \mathbf{k} (the corresponding energy is $E = c\sqrt{c^2 + k^2}$) and the polarization μ in the far future. This function can be written as [60–62]

$$\begin{aligned} \Psi_{\mathbf{k}\mu}^-(\mathbf{r}) &= \frac{1}{\sqrt{4\pi}} \frac{c}{\sqrt{Ek}} \sum_{\kappa m_j} C_{l0,1/2\mu}^{j\mu} i^l \\ &\times \sqrt{2l+1} e^{-i\delta_{\kappa}} D_{m_j\mu}^j(\mathbf{z} \rightarrow \mathbf{k}) \Psi_{E\kappa m_j}(\mathbf{r}). \end{aligned} \quad (14)$$

Here κ is the relativistic quantum number, $j = |\kappa| - 1/2$, $l = j + \frac{1}{2} \text{sgn}(\kappa)$, $C_{l0,1/2\mu}^{j\mu}$ is the Clebsch-Gordan coefficient, and $D_{m_j\mu}^j(\mathbf{z} \rightarrow \mathbf{k})$ is the Wigner matrix rotating the z axis into

the \mathbf{k} direction [63]. The eigenfunctions of the Hamiltonian H_0 are normalized on the energy scale and take the form

$$\Psi_{E\kappa m_j}(\mathbf{r}) = \frac{1}{r} \begin{pmatrix} g_{\kappa}(r) \Omega_{\kappa m}(\mathbf{n}) \\ i f_{\kappa}(r) \Omega_{-\kappa m}(\mathbf{n}) \end{pmatrix}, \quad (15)$$

where $\Omega_{\kappa m}(\mathbf{n})$ is the spherical bispinor, and $\mathbf{n} = \mathbf{r}/r$. In the present work the radial functions $g_{\kappa}(r)$ and $f_{\kappa}(r)$ along with the scattering phase shifts δ_{κ} are obtained numerically using the modified RADIAL package [64]. The full continuum wavefunction is normalized as follows:

$$\langle \Psi_{\mathbf{k}\mu}^-(\mathbf{r}) | \Psi_{\mathbf{k}'\mu}^-(\mathbf{r}) \rangle = \delta(\mathbf{k} - \mathbf{k}'). \quad (16)$$

C. Relativistic Volkov functions within the dipole approximation

In the original paper [65], analytical solutions of the Dirac equation were introduced in case of the external field in the form of a plane wave. In the non-relativistic case Volkov functions within the dipole approximation can be built by propagation of the plane waves from $-\infty$ to the moment in time τ with the analytical propagator

$$U^{\text{V,NR}}(\tau, -\infty) = \exp \left(-\frac{i}{2} \int_{-\infty}^{\tau} dt (\mathbf{k} + \mathbf{A}(t))^2 \right); \quad (17)$$

the analytical Volkov-type approximate solutions also can be built beyond the dipole approximation [66]. However, the “dipole” Volkov functions for the Dirac equations do not have closed-form expressions. It can be shown though, that the Volkov functions can be constructed with the numerical solution of the second-order differential equation for a scalar function [67, 68]. Here we will follow the procedure from Ref. [68].

We start with the Dirac equation with the pure electric external field $\mathbf{F}(t) = -\frac{\partial}{\partial t} \mathbf{A}(t)$:

$$\left(i\beta \frac{\partial}{\partial t} - c\beta \boldsymbol{\alpha} \cdot (\mathbf{p} + \mathbf{A}(t)) - c^2 \right) \chi(\mathbf{r}, t) = 0. \quad (18)$$

Substituting the solution χ in the form

$$\chi(\mathbf{r}, t) = \left(i\beta \frac{\partial}{\partial t} - c\beta \boldsymbol{\alpha} \cdot (\mathbf{p} + \mathbf{A}(t)) - c^2 \right) \phi(\mathbf{r}, t), \quad (19)$$

supposing $p_y = 0$ without loss of generality, and assuming the vector potential to be directed along the z axis, we get:

$$\begin{aligned} & \frac{\partial^2 \phi(\mathbf{r}, t)}{\partial t^2} - icF(t) \alpha_z \phi(\mathbf{r}, t) + c^2 p_x^2 \alpha_x^2 \phi(\mathbf{r}, t) \\ & + c^2 (p_z + A(t))^2 \alpha_z^2 \phi(\mathbf{r}, t) - c^4 \phi(\mathbf{r}, t) = 0. \end{aligned} \quad (20)$$

The solution of the Eq. (20) can be written in the form:

$$\phi_{\mathbf{k}qs}(\mathbf{r}, t) = \phi_{\mathbf{k}s}(t) \exp(i\mathbf{k} \cdot \mathbf{r}) v_{s,q}, \quad s = \pm 1, q = \pm 1, \quad (21)$$

where the constant orthonormal spinors $v_{s,q}$ ($v_{s,q}^\dagger v_{s',q'} = \delta_{qq'}$) satisfy the following equations:

$$\alpha_z v_{s,q} = s v_{s,q}; \quad \beta \alpha_x v_{s,q} = i q v_{s,q}. \quad (22)$$

From Eqs. (20)-(22) one can obtain the following equation for the scalar function $\phi_{\mathbf{k}s}(t)$:

$$\left(\frac{d^2}{dt^2} + c^2(k_z + A(t))^2 + c^2k_x^2 - i\text{sc}F(t) + c^4 \right) \phi_{\mathbf{k}s}(t) = 0. \quad (23)$$

The equation (23) has two independent solutions, corresponding to the sign of the particle energy $\pm E = \pm c\sqrt{c^2 + k^2}$ (i.e. to the particle (+) and antiparticle (-)) [67] before the interaction with the external field is switched on. For the commonly used laser field parameters we can neglect the possible transitions between the negative and positive continua (i.e. pair creation in an electromagnetic field), and use only the solution corresponding to the positive continuum:

$$i \frac{d}{dt} \phi_{\mathbf{k}s}(t) = E \phi_{\mathbf{k}s}(t), \quad t \rightarrow -\infty. \quad (24)$$

Also since the solutions with fixed r , \mathbf{k} and different s are linearly dependent [68], only the independent functions $\phi_{\mathbf{k}1}(t) \equiv \phi_{\mathbf{k}}(t)$ should be considered.

The ordinary differential equation (23) can be efficiently solved numerically by the implicit Runge-Kutta method. The number of such equations, however, can be quite large depending on the desired momentum \mathbf{k} resolution. Having the values $\phi_{\mathbf{k}}(t_j)$ with their derivatives, the set of the Volkov functions can be constructed as follows:

$$\chi_{\mathbf{k}q}^{\text{V}}(t_j) = -\frac{1}{4\pi^{3/2}} e^{i\mathbf{k} \cdot \mathbf{r}} \begin{pmatrix} -iq\alpha_{\mathbf{k}q}(t_j) \\ \alpha_{\mathbf{k}q}(t_j) \\ iq\beta_{\mathbf{k}q}(t_j) \\ \beta_{\mathbf{k}q}(t_j) \end{pmatrix}, \quad (25)$$

where

$$\alpha_{\mathbf{k}q}(t) = i \frac{d}{dt} \phi_{\mathbf{k}}(t) + (c^2 - c(k_z + A(t)) - iqck_x) \phi_{\mathbf{k}}(t), \quad (26)$$

$$\beta_{\mathbf{k}q}(t) = i \frac{d}{dt} \phi_{\mathbf{k}}(t) + (-c^2 - c(k_z + A(t)) + iqck_x) \phi_{\mathbf{k}}(t), \quad (27)$$

Note that one should normalize the initial conditions for the Eq. (23) to provide

$$\frac{1}{2} [|\alpha_{\mathbf{k}q}(0)|^2 + |\beta_{\mathbf{k}q}(0)|^2] = |\dot{\phi}_{\mathbf{k}}(0)|^2 + E^2 |\phi_{\mathbf{k}}(0)|^2 \quad (28)$$

$$+ 2ck_z \text{Im}(\dot{\phi}_{\mathbf{k}}(0)\phi_{\mathbf{k}}^*(0)) = 1$$

in order to make the set of Volkov functions (25) orthonormal (for completeness the negative energy solutions should also be included in the set).

D. Relativistic mask method

Analogous to the non-relativistic mask method [36–38], the whole coordinate space is divided into the inner (I) and outer (II) parts. Within the inner region, the wavefunction is propagated numerically with the method described in Sec. II A with

the full Hamiltonian. In the outer region, we neglect the interaction with the nucleus and make use of the Volkov states propagation in the momentum representation.

Let us consider the j 's step of the time propagation. At this step the wavefunction, which is a result of the propagation from the previous step in the inner region, should be divided in two parts by a smooth mask function $M(r)$ (“absorber”), which is equal to unity for $r < R$, and decreases to zero at some point R_{max} :

$$\Psi(\mathbf{r}, t_j) = \underbrace{M(r) \cdot \Psi(\mathbf{r}, t_j)}_{\Psi_{\text{I}}} + \underbrace{(1 - M(r)) \cdot \Psi(\mathbf{r}, t_j)}_{\Psi_{\text{II}}}. \quad (29)$$

After that the numerical propagation according to the scheme (11) continues only for the inner part Ψ_{I} step by step (with the procedure (29) performed on each step) to some moment in time $\tau > T$. The value of τ should be large enough (typically, several optical cycles) so the absorber could “capture” the whole ionized wavepacket. As a result, the normalization integral within the sphere of radius R

$$N(t) = \int_{r \leq R} d\mathbf{r} \langle \Psi(\mathbf{r}, t) | \Psi(\mathbf{r}, t) \rangle \quad (30)$$

is decreasing with time. Given that the value of R is large enough, the quantity $P = 1 - N(\tau)$ after the end of the laser pulse T can be interpreted as the ionization probability.

Note that the wavefunction splitting by the procedure (29) does not allow the parts of the ionized wavepacket to move back from the outer to the inner region, so one should ensure that the value of R at least exceeds the electron excursion in the oscillating laser field. The final results should be checked in terms of convergence with respect to R . The value $R_{\text{max}} - R$, i.e. the width of the absorber, can also influence the final results (see Ref. [39] for the detailed discussion), so the convergence should be checked with respect to this quantity as well.

The absorbed outer parts ($\{\Psi_{\text{II}}(t_j)\}$) of the wavefunction are used to calculate the following scalar products:

$$C_j^q(\mathbf{k}) = \langle \chi_{\mathbf{k}q}^{\text{V}}(t_j) | \Psi_{\text{II}}(t_j) \rangle, \quad (31)$$

where $\chi_{\mathbf{k}q}^{\text{V}}(t_j)$ is the Volkov function (25).

Finally, the differential ionization probability for the electrons emitted with the momentum \mathbf{k} into the unit energy and solid angle intervals is evaluated as:

$$\frac{d^2 P(\mathbf{k})}{dE d\Omega} = \frac{1}{c^2} E k \sum_q \left| \sum_j C_j^q(\mathbf{k}) \right|^2. \quad (32)$$

The photoelectron energy spectrum can be obtained by integration of PAD (32) over the angles:

$$\frac{dP(E)}{dE} = \int \frac{dP(\mathbf{k})}{dE d\Omega} d\Omega. \quad (33)$$

Then the additional integration of the spectrum (33) over the emitted electron energy can be performed to obtain the ionization probability P :

$$P = \int_0^\infty \frac{dP(E)}{dE} dE. \quad (34)$$

The comparison of the total ionization probability obtained with Eq. (34) with the same quantity evaluated as $1 - N(\tau)$ is used to control the accuracy of the results.

III. NUMERICAL EXAMPLES AND DISCUSSION

To demonstrate the implementation of the relativistic mask method (RMM), we evaluate the PAD using two different ionization scenarios: multiphoton ionization of the Xe^{53+} ion and over-the-barrier ionization of the hydrogen atom in superstrong laser fields. Since the chosen external fields in both cases possess high peak intensities and short wavelengths, we discuss the applicability of the dipole approximation first. As we mentioned in the Introduction, two conditions should be satisfied. The first one is smallness of the characteristic size of the target r_{ion} (measured as the mean distance of the electron from the nucleus in the ground state) with respect to the laser wavelength λ . The dipole approximation is expected to work well if $\lambda/r_{\text{ion}} \gg 1$. In our calculations (see the external field parameters below), $\lambda/r_{\text{ion}} \sim 100$ for the first example (Xe^{53+}), and $\lambda/r_{\text{ion}} \sim 250$ for the second one (H atom). The second condition assumes displacement of the classical electron due to the magnetic force in the direction perpendicular to that of the field polarization to be small compared to the electron wavepacket width at the moment of electron-target recollision. This condition is satisfied if $\Gamma_R \ll 1$, where Γ_R is the Lorentz deflection parameter [46]:

$$\Gamma_R = \frac{\sqrt{I_p U_p^3}}{3\omega c^2}. \quad (35)$$

In Eq. (35), I_p is the ionization potential of the target and $U_p = F^2/(4\omega^2)$ is the ponderomotive potential. In our calculations, $\Gamma_R \sim 10^{-4}$ and $\Gamma_R \sim 10^{-5}$ for the first and second case studies, respectively. At the end of this brief discussion, we may conclude that no significant difference between the present results and those obtained beyond the dipole approximation is expected for the parameters used in the calculations. Since the magnetic field effects scale as v/c (v is the characteristic electron velocity) while the other relativistic effects (like the mass correction) scale as v^2/c^2 at most, we do not expect large relativistic effects due to the external field (where $v \sim F/\omega$) either. However, the relativistic effects in the initial state of the heavy hydrogen-like ion (Xe^{53+}), such as a relativistic change of the ionization potential, are important and fully included in the solution of the Dirac equation.

A. Multiphoton ionization of the H-like Xe ion

As an example demonstrating applicability and performance of the RMM method, we evaluate the PAD for the H-like Xe ($Z = 54$) ion after multiphoton above-threshold ionization (ATI) by a linearly-polarized laser pulse with the sin-squared envelope containing 20 optical cycles. The carrier wavelength is 0.1 nm (the corresponding photon energy is 455.63 a.u.) and the laser peak intensity is set to 8×10^{23}

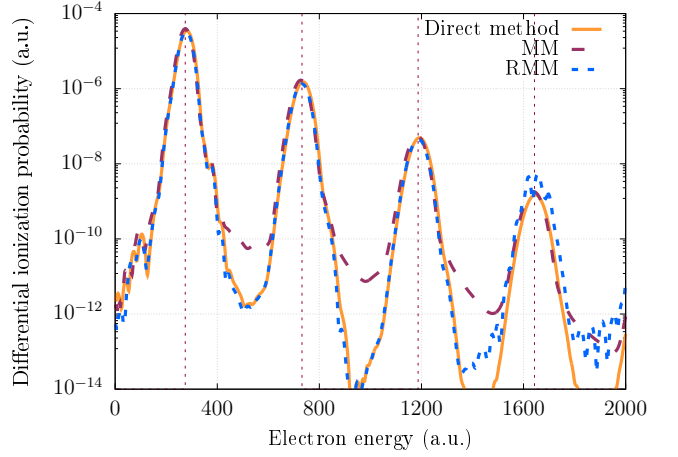


Figure 1. Photoelectron spectra for the Xe^{53+} ion exposed to a linearly-polarized laser pulse. Carrier wavelength is 0.1 nm, peak intensity is 8×10^{23} W/cm². The pulse contains 20 optical cycles. Different curves correspond to the different way of the spectra evaluation.

W/cm². The Keldysh parameter [69] γ is equal to 5.26, which corresponds to the multiphoton ionization regime.

For comparison, we also show the results obtained with the usual non-relativistic mask method (MM) for the artificial ion with a value of $Z = 55.13$, which gives the same ionization potential as the original ion and allows us to capture the major quantitative part of the relativistic effects in the considered process [13, 18].

The photoelectron spectra calculated with different approaches are shown in Fig. 1. The vertical dashed lines represent the approximate positions of the peaks calculated as

$$E_n = -I_p + n\omega - U_p, \quad (36)$$

where the ionization potential I_p is equal to 1519.47 a.u. for Xe^{53+} , and n is the number of absorbed photons (for the process under consideration, $n \geq 4$). One can see in Fig. 1 that RMM successfully reproduces the spectra calculated with both the direct method and the non-relativistic treatment. However, the numerical simulation box with the linear dimension of 5 a.u. is sufficient for the RMM calculations while the direct method requires the box size twice as large.

Angular distributions calculated directly and with the RMM are depicted in Fig. 2. The results are in good agreement here as well. Angular structure of the rings can be understood in terms of the dominant angular momentum of the photoelectrons [70], namely, the number of nodes is equal to the dominant value of the angular momentum in the continuum state. The first ring corresponds to the absorption of 4 photons, so it may contain contributions from the angular momenta 0, 2, and 4. The dominant value of the angular momentum is equal to 2, as one can infer from the node structure of the first ring in Fig. 2.

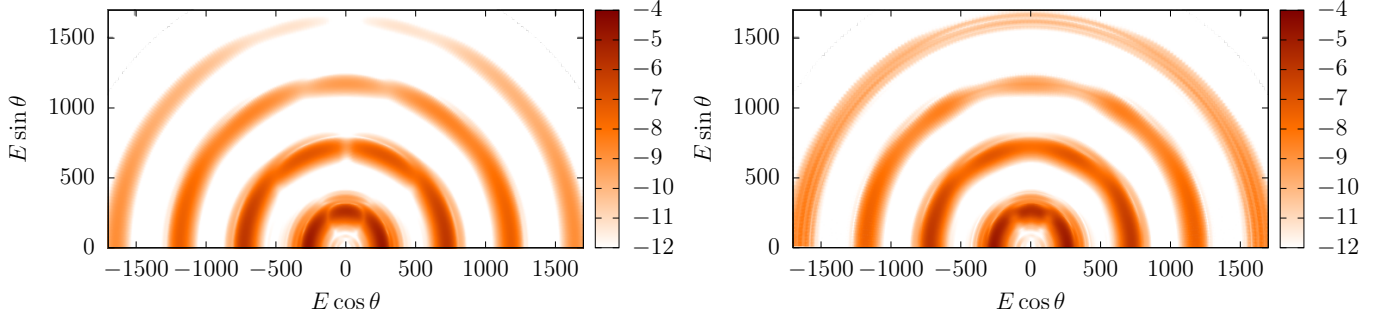


Figure 2. Two-dimensional energy-angular distributions for the Xe^{53+} ion exposed to a linearly-polarized laser pulse calculated with the direct method (left) and with the relativistic mask method (right). Carrier wavelength is 0.1 nm, peak intensity is $8 \times 10^{23} \text{ W/cm}^2$. The pulse contains 20 optical cycles. The PAD intensity scale is logarithmic and shown as a color map.

B. Electron distributions after ionization of hydrogen atom in a superstrong laser field

Here we study ionization of a hydrogen atom by a short linearly-polarized pulse of electromagnetic radiation with the carrier wavelength 13 nm (photon energy 3.5 a.u.). The pulse envelope has a \sin^2 shape with the peak intensity $3.5 \times 10^{18} \text{ W/cm}^2$ and contains 5 optical cycles. Since the ionization potential of the hydrogen atom is equal to 0.5 a.u., we have an ionization regime where both the photon energy essentially (about 7 times) exceeds the ionization potential and the peak value of the external field exceeds by far (about 19 times) the Coulomb force from the nucleus on the first Bohr orbit.

The results of our calculations are presented in Fig. 3. One can clearly see two ATI peaks, the first one centered around 2.8 a.u., and the second one around 6.3 a.u. The RMM and direct method results agree very well. To capture the “slow” electrons with the mask method, one should propagate the wavefunction for a long time after the interaction with the laser. We avoid this by calculating the low-energy structure with the direct method, thus a hybrid method is eventually used with the two different techniques applied on different energy ranges.

Note that the ponderomotive potential is very large for this superstrong field: $U_p = 2$ a.u. According to Eq. (36), one should observe a large shift (comparable with the peak spacing) in the positions of the ATI peaks. Clearly this is not the case, as one can see in Fig. 3. Moreover, the ATI peak positions have only very weak dependence on the laser field intensity (the “weaker field” curve in Fig. 3 corresponding to the peak intensity of $2.3 \times 10^{18} \text{ W/cm}^2$ is slightly shifted to the left), again in contradiction with Eq. (36). A breakdown of Eq. (36) in superstrong laser fields, however, can be easily understood. The formula (36) for the positions of the ATI peaks is based on a simple and intuitive picture: while the continuum and weakly bound states are strongly perturbed by the external oscillating field, and their energies are shifted by the mean oscillation energy U_p , the tightly bound ground state is perturbed only weakly, and its energy remains unchanged (if one neglects the relatively small ac Stark shift). Therefore the ionization potential is effectively increased by U_p , and one

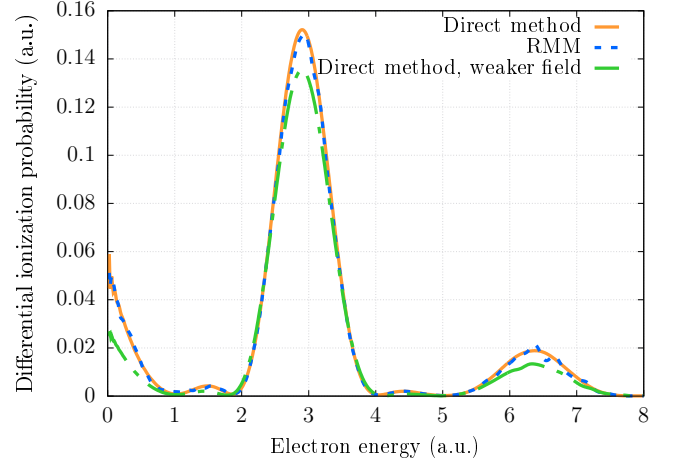


Figure 3. Photoelectron spectra for the hydrogen atom exposed to a linearly-polarized laser pulse with the duration of 5 optical cycles. The carrier wavelength is 13 nm and the peak intensity is $3.5 \times 10^{18} \text{ W/cm}^2$ (except for “weaker field” curve, which corresponds to the peak intensity of $2.3 \times 10^{18} \text{ W/cm}^2$). The methods used to evaluate the spectra are as labeled.

can observe the ATI peaks moving towards lower energies and even change in the minimum number of photons required for ionization (peak switching [23]), as the intensity of the laser field becomes higher. When the field becomes superstrong, however, this picture changes dramatically. In a superstrong external field, not only the continuum and weakly bound states but also tightly bound states, including the ground state, are strongly perturbed by the field. Now all the states, bound and continuum, are shifted by the same amount of energy, U_p . Hence the ionization potential does not change compared to the case of the weak external field where both U_p and ac Stark shift are small. Therefore in a superstrong field one can see the ATI peaks approximately at the same positions as in a relatively weak laser field, that is, not shifted by the ponderomotive potential.

The two-dimensional energy-angle spectra calculated with the direct method (and reproduced with the mask method) are

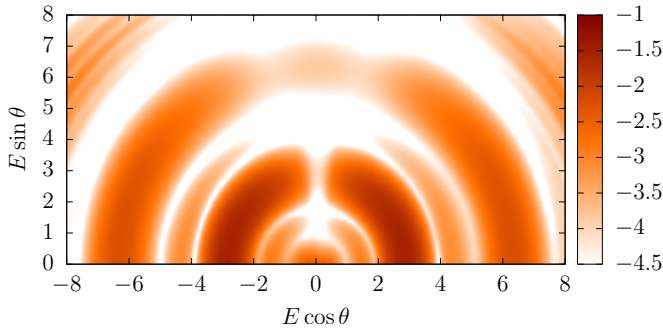


Figure 4. Two-dimensional energy-angle distribution for the hydrogen atom exposed to a linearly-polarized laser pulse. Carrier wavelength is 13 nm, peak intensity is 3.5×10^{18} W/cm². The pulse contains 5 optical cycles. The PAD intensity scale is logarithmic and shown as a color map.

presented in Fig. 4. One can see slight forward-backward asymmetry, what is usually the case for the short pulses. The main one- and two-photon absorption rings are accompanied by weaker satellites. This multiring oscillatory structure within the ATI peak is due to interference of the electronic signal coming from the leading and trailing edges of the laser pulse [28].

IV. CONCLUSION

In this contribution, we have extended the mask (or wavefunction-splitting) method for evaluation of the photoelectron energy spectra and angular distributions to the relativistic domain within the dipole approximation. Despite the dipole approximation lacks analytical closed-form expressions for the relativistic Volkov states, a set of uncoupled second-order ordinary differential equations for a scalar function can be efficiently solved to construct such states numerically. Quantum electrodynamics effects are neglected in the present study because the electromagnetic fields used in the calculations are not strong enough to make these effects significant for the processes under consideration.

To demonstrate the implementation of the method, we

have performed two case studies, both within the dipole approximation: multiphoton above-threshold ionization of the hydrogen-like Xe^{53+} ion and ionization of the hydrogen atom in a superstrong electromagnetic field. The ionization regimes in these two cases are considerably different. Nonetheless, in both cases the relativistic mask method is able to reproduce the electron energy and angular distributions calculated with the direct approach, that is by projecting the final wavefunction onto the continuum states of the target ion. Although the direct method is straightforward to implement, it has evident limitations. This method may have serious difficulties in evaluation of the spectra of fast photoelectrons, which may leave the simulation box before the laser field is switched off. For the same reason, longer pulses are not well-suited for the direct method either. Certainly, these difficulties can be avoided by expansion of the simulation box, but this will result in more demanding and heavy computations. In this respect, the relativistic mask method is more robust and efficient since it can catch the fast electrons “on the fly” before they leave the box, so a huge simulation box is not required. Although in the present formulation the relativistic mask method is restricted to the dipole approximation, we believe it can find its applications, for example, in comparison with the full nondipole calculations for estimation of the nondipole effects.

V. AUTHORS CONTRIBUTIONS

D. A. Tumakov carried out the numerical calculations. All the authors were involved in discussions and preparation of the manuscript. All the authors have read and approved the final manuscript.

ACKNOWLEDGMENTS

This work was supported by Russian Foundation for Basic Research (Grant No. 20-02-00199). D. A. Tumakov acknowledges the support from TU Dresden (DAAD-Programm Ostpartnerschaften). The calculations were performed at the Computing Center of SPbSU Research Park.

-
- [1] T. Brabec and F. Krausz, *Rev. Mod. Phys.* **72**, 545 (2000).
 - [2] P. Agostini and L. F. DiMauro, *Reports on Progress in Physics* **67**, 813 (2004).
 - [3] F. Krausz and M. Ivanov, *Rev. Mod. Phys.* **81**, 163 (2009).
 - [4] A. Di Piazza, C. Müller, K. Z. Hatsagortsyan, and C. H. Keitel, *Rev. Mod. Phys.* **84**, 1177 (2012).
 - [5] T. Tschentscher and R. Feidenhans'l, *Synchrotron Radiat. News* **30**, 21 (2017).
 - [6] M. Dunne and B. Schoenlein, *Synchrotron Radiat. News* **30**, 7 (2017).
 - [7] M. Vogel, W. Quint, G. Paulus, and T. Stöhlker, *Nuclear Instruments and Methods in Physics Research Section B: Beam Interactions with Materials and Atoms* **285**, 65 (2012).
 - [8] S. Ringleb, M. Vogel, S. Kumar, W. Quint, G. G. Paulus, and T. Stöhlker, *Physica Scripta* **T166**, 014067 (2015).
 - [9] N. Stallkamp, S. Ringleb, B. Arndt, M. Kiffer, S. Kumar, T. Morgenroth, G. Paulus, W. Quint, T. Stöhlker, and M. Vogel, *X-Ray Spectrometry* **49**, 188 (2020).
 - [10] M. Klaiber, E. Yakaboylu, and K. Z. Hatsagortsyan, *Phys. Rev. A* **87**, 023417 (2013).
 - [11] H. Bauke, H. G. Hetzheim, G. R. Mocken, M. Ruf, and C. H. Keitel, *Phys. Rev. A* **83**, 063414 (2011).
 - [12] F. Fillion-Gourdeau, E. Lorin, and A. D. Bandrauk, *Computer Physics Communications* **183**, 1403 (2012).
 - [13] Y. V. Vanne and A. Saenz, *Phys. Rev. A* **85**, 033411 (2012).

- [14] D. A. Telnov, K. E. Sosnova, E. Rozenbaum, and S.-I. Chu, *Phys. Rev. A* **87**, 053406 (2013).
- [15] E. B. Rozenbaum, D. A. Glazov, V. M. Shabaev, K. E. Sosnova, and D. A. Telnov, *Phys. Rev. A* **89**, 012514 (2014).
- [16] I. A. Ivanov, *Phys. Rev. A* **91**, 043410 (2015).
- [17] T. Kjellsson, S. Selstø, and E. Lindroth, *Phys. Rev. A* **95**, 043403 (2017).
- [18] I. V. Ivanova, V. M. Shabaev, D. A. Telnov, and A. Saenz, *Phys. Rev. A* **98**, 063402 (2018).
- [19] T. K. Lindblom, M. Førre, E. Lindroth, and S. Selstø, *Phys. Rev. Lett.* **121**, 253202 (2018).
- [20] P. Agostini, F. Fabre, G. Mainfray, G. Petite, and N. K. Rahman, *Phys. Rev. Lett.* **42**, 1127 (1979).
- [21] P. B. Corkum, Plasma perspective on strong field multiphoton ionization, *Phys. Rev. Lett.* **71**, 1994 (1993).
- [22] H. G. Muller, A. Tip, and M. J. van der Wiel, *J. Phys. B: Atomic and Molecular Physics* **16**, L679 (1983).
- [23] P. Kruit, J. Kimman, H. G. Muller, and M. J. van der Wiel, *Phys. Rev. A* **28**, 248 (1983).
- [24] R. R. Freeman, P. H. Bucksbaum, H. Milchberg, S. Darack, D. Schumacher, and M. E. Geusic, *Phys. Rev. Lett.* **59**, 1092 (1987).
- [25] R. M. Potvliege and S. Vučić, *J. Phys. B: Atomic and Molecular Physics* **42**, 055603 (2009).
- [26] C. I. Blaga, F. Catoire, P. Colosimo, G. G. Paulus, H. G. Muller, P. Agostini, and L. F. DiMauro, *Nature Physics* **5**, 335 (2009).
- [27] C. Liu and K. Z. Hatsagortsyan, *Phys. Rev. Lett.* **105**, 113003 (2010).
- [28] D. A. Telnov and S.-I. Chu, *J. Phys. B* **28**, 2407 (1995).
- [29] F. Lindner, M. G. Schätzel, H. Walther, A. Baltuška, E. Goulielmakis, F. Krausz, D. B. Milošević, D. Bauer, W. Becker, and G. G. Paulus, *Phys. Rev. Lett.* **95**, 040401 (2005).
- [30] M. Wickenhauser, X. M. Tong, and C. D. Lin, *Phys. Rev. A* **73**, 011401(R) (2006).
- [31] D. G. Arbó, E. Persson, and J. Burgdörfer, *Phys. Rev. A* **74**, 063407 (2006).
- [32] D. G. Arbó, K. L. Ishikawa, K. Schiessl, E. Persson, and J. Burgdörfer, *Phys. Rev. A* **81**, 021403(R) (2010).
- [33] D. G. Arbó, K. L. Ishikawa, K. Schiessl, E. Persson, and J. Burgdörfer, *Phys. Rev. A* **82**, 043426 (2010).
- [34] D. A. Tumakov, D. A. Telnov, G. Plunien, and V. M. Shabaev, *Phys. Rev. A* **100**, 023407 (2019).
- [35] K. J. Schafer and K. C. Kulander, *Phys. Rev. A* **42**, 5794 (1990).
- [36] S. Chelkowski, C. Foisy, and A. D. Bandrauk, *Phys. Rev. A* **57**, 1176 (1998).
- [37] X. M. Tong, K. Hino, and N. Toshima, *Phys. Rev. A* **74**, 031405(R) (2006).
- [38] U. De Giovannini, D. Varsano, M. A. L. Marques, H. Appel, E. K. U. Gross, and A. Rubio, *Phys. Rev. A* **85**, 062515 (2012).
- [39] U. De Giovannini, A. H. Larsen, and A. Rubio, *European Physics Journal B* **88**, 56 (2015).
- [40] D. A. Telnov and S.-I. Chu, *Phys. Rev. A* **79**, 043421 (2009).
- [41] D. A. Telnov and S.-I. Chu, *Phys. Rev. A* **83**, 063406 (2011).
- [42] L. Tao and A. Scrinzi, *New J. Phys.* **14**, 013021 (2012).
- [43] Z. Zhou and S.-I. Chu, *Phys. Rev. A* **83**, 013405 (2011).
- [44] Z. Zhou and S.-I. Chu, *Phys. Rev. A* **87**, 023407 (2013).
- [45] H. R. Reiss, *Phys. Rev. A* **63**, 013409 (2001).
- [46] S. Palaniyappan, I. Ghebregziabher, A. DiChiara, J. MacDonald, and B. C. Walker, *Phys. Rev. A* **74**, 033403 (2006).
- [47] H. R. Reiss, *Phys. Rev. Lett.* **101**, 043002 (2008).
- [48] A. Ludwig, J. Maurer, B. W. Mayer, C. R. Phillips, L. Gallmann, and U. Keller, *Phys. Rev. Lett.* **113**, 243001 (2014).
- [49] M. Klaiber, K. Z. Hatsagortsyan, J. Wu, S. S. Luo, P. Grugan, and B. C. Walker, *Phys. Rev. Lett.* **118**, 093001 (2017).
- [50] I. Angeli and K. Marinova, *Atomic Data and Nuclear Data Tables* **99**, 69 (2013).
- [51] G. Yao and S. I. Chu, *Chem. Phys. Lett.* **204**, 381 (1993).
- [52] D. A. Telnov and S. I. Chu, *Phys. Rev. A* **59**, 2864 (1999).
- [53] V. F. Bratzev, G. B. Deyneka, and I. I. Tupitsyn, *Bull. Acad. Sci. USSR, Phys. Ser* **41**, 173 (1977).
- [54] G. W. F. Drake and S. P. Goldman, *Phys. Rev. A* **23**, 2093 (1981).
- [55] X. M. Tong and S. I. Chu, *Chem. Phys.* **217**, 119 (1997).
- [56] D. A. Tumakov, D. A. Telnov, I. A. Maltsev, G. Plunien, and V. M. Shabaev, *Nuclear Instruments and Methods in Physics Research Section B: Beam Interactions with Materials and Atoms* **408**, 276 (2017).
- [57] D. A. Telnov, D. A. Krapivin, J. Heslar, and S.-I. Chu, *The Journal of Physical Chemistry A* **122**, 8026 (2018).
- [58] J. Crank and P. Nicolson, *Mathematical Proceedings of the Cambridge Philosophical Society* **43**, 50–67 (1947).
- [59] <https://software.intel.com/en-us/articles/intel-mkl-pardiso>.
- [60] M. E. Rose, *Elementary theory of angular momentum* (Courier Corporation, 1995).
- [61] J. Eichler and T. Stöhlker, *Physics Reports* **439**, 1 (2007).
- [62] V. A. Zaytsev, S. Tashenov, A. V. Maiorova, V. M. Shabaev, and T. Stöhlker, *J. Phys. B: Atomic, Molecular and Optical Physics* **48**, 165003 (2015).
- [63] D. A. Varshalovich, A. N. Moskalev, and V. K. Khersonskii, *Quantum theory of angular momentum* (World Scientific, 1988).
- [64] F. Salvat, J. Fernández-Varea, and W. Williamson, *Computer Physics Communications* **90**, 151 (1995).
- [65] D. M. Wolkow, *Zeitschrift für Physik* **94**, 250 (1935).
- [66] B. Böning, W. Paufler, and S. Fritzsche, *Phys. Rev. A* **99**, 053404 (2019).
- [67] E. S. Fradkin, D. M. Gitman, and S. M. Shvartsman, *Quantum electrodynamics with unstable vacuum* (Springer Berlin, 1991).
- [68] S. P. Gavrilov and D. M. Gitman, *Phys. Rev. D* **53**, 7162 (1996).
- [69] L. V. Keldysh, *Sov. Phys. - JETP* **20**, 1307 (1965).
- [70] Z. Chen, T. Morishita, A.-T. Le, M. Wickenhauser, X. M. Tong, and C. D. Lin, *Phys. Rev. A* **74**, 053405 (2006).